Stresses about a Circular Hole in a Cylindrical Shell

PETER VAN DYKE*
Martin Company, Baltimore, Md.

The effects of a circular hole on the initial states of uniform stress produced by loading an infinite shallow cylindrical shell by axial tension, internal pressure, and torsion are determined. Manipulation of the linear equations as defined for thin, shallow cylindrical shells yields a single complex differential equation involving the dimensionless parameter β; the solution of the equation is obtained for three ranges of this curvature parameter. A starting solution for the stresses involves a perturbation in the parameter β; the results to terms of order β^2, first obtained by Lurie for the membrane stresses due to loading by axial tension and internal pressure, are corrected. The solution of the governing differential equation as an infinite series of Hankel functions is used to obtain values of the membrane and bending stresses for intermediate values of β under the three loading conditions. The series solution is terminated at a finite number of terms and satisfies the boundary conditions by a collocation procedure. The behavior of the stresses for large values of β is estimated for the shell loaded by axial tension and internal pressure by employing boundary-layer techniques. Comparisons are made between these results and other theoretical work as well as with available experimental data.

Introduction

THIS paper is concerned with obtaining stresses occurring about a circular hole cut in a cylindrical shell. Three loadings of the shell are considered: loading by axial tension, internal pressure, and torsion; stresses are found both at the hole edge and in the shell interior. For the pressure case, the hole is considered to be covered by a diaphragm that allows the hole edge to deflect and rotate but transmits the pressure force to the shell in the form of a uniform transverse shear stress at the hole edge.

The shell configuration is shown in Fig. 1. The principal dimensions a, R, and t are indicated as follows: a is the radius of the circular hole; R is the radius of curvature of the shell middle surface; and t is the uniform shell thickness. A single parameter, the curvature parameter β, defined in terms of these quantities will be seen to enter the problem. It is defined as

$$\beta^2 = a^2[12(1 - \nu^2)]^{1/2}/8\,Rt \tag{1}$$

The region of the cylindrical shell which contains the hole will be treated by shallow shell theory. A shallow cylindrical shell may be described as a shell whose ratio of rise to base length is small, which implies that its circumferential dimension is small compared with its radius of curvature. By limiting the ratio of the hole radius to the radius of curvature a/R the effects of the hole may be confined to an area that is within a small radial distance from the hole; this region of the shell may be considered to be a shallow shell. In addition, the shell thickness must remain small, as dictated by the use of a shallow, thin shell theory.

The first attempt to obtain a solution for the case of a circular hole cut in a cylindrical shell was made in 1947 by Lurie[1] for loading by axial tension and internal pressure. The method of solution involved a perturbation in the curvature parameter β and extended through terms of order β^2. The solutions, which are valid only for small values of β, reduce to the flat-plate solutions for β equal to zero. By a similar perturbation method, Shevliakov and Zigel[2] obtained a solution for small β for the problem of torsion loading. The first extension of the results for shells with larger values of the curvature parameter was made in 1958 by Withum[3] for the problem of the shallow cylindrical shell with a circular hole loaded by torsion. A perturbation technique was employed to obtain the stresses in the shell for values of the curvature parameter up to 2. More recently, Eringen and his co-workers[4] and Lekkerkerker[5] have employed numerical procedures to obtain the stresses in the shell for the three loading conditions; Eringen also extended Withum's method to the problem of loading by internal pressure. Each term in a Fourier series solution satisfied the hole boundary conditions in Lekkerkerker's solution, while Eringen employed a collocation procedure similar to the numerical collocation procedure used in this paper. The work of Lekkerkerker proceeded simultaneously with that of this paper, and Eringen's results were not discovered until the calculations for the stresses at the hole had been completed. The analyses of both of these investigators extended to a β of about 1.75 whereas the numerical calculations included in this report extend to a β of 4.

Received December 9, 1964; revision received May 14, 1964. This work was sponsored by the Office of Naval Research under Contract No. Nonr 1866(02) with Harvard University. The author is indebted to Bernard Budiansky of Harvard University for inspiring and directing this work.

* Engineering Specialist. Member AIAA.

Formulation of the Problem

The equations that are considered to govern the behavior of the region of the shell which is influenced by the presence of the hole are the shallow, thin shell equations. These equations have been written in general, nonlinear form by Marguerre;[6] they are specialized here to the linear equations for the case of a cylindrical geometry. The stress conditions in the shell, as described by the stress resultants and the displacements tangential and normal to the middle surface, are shown in Fig. 2.

The linear shallow shell equations for a cylindrical shell geometry may be readily combined into two differential equations involving only the membrane stress function F and the normal displacement W. These two equations are

$$\nabla^4 F + F_{,xx}/RD = p/D \tag{2}$$

and

$$\nabla^4 F - tE\,W_{,xx}/R = 0 \tag{3}$$

where

$$D = Et^3/12(1 - \nu^2) \tag{4}$$

and

$$W_{,x} = \partial W/\partial x \qquad \nabla^4 W = \nabla^2(\nabla^2 W) = W_{,xxxx} + 2W_{,xxyy} + W_{,yyyy} \tag{5}$$

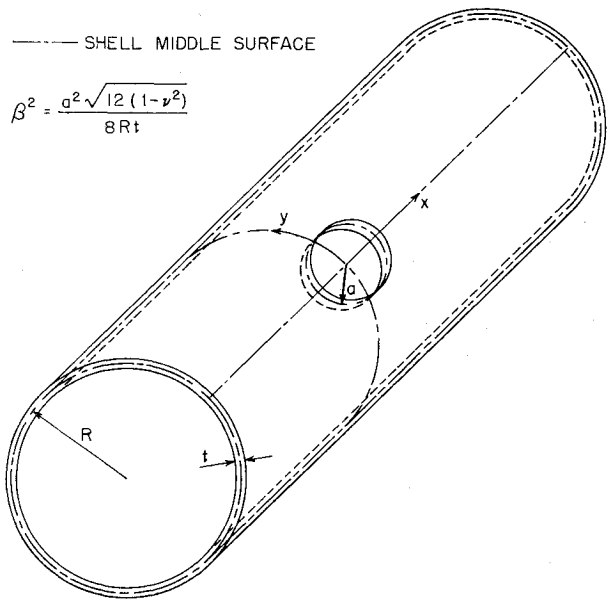

Fig. 1 Cylindrical shell configuration.

A distributed load normal to the middle surface is given by p, and the two material properties are the modulus of elasticity E and Poisson's ratio ν.

A process of nondimensionalization of the system of equations is now carried out. The nondimensional coordinates ξ and η are defined in terms of the dimensional coordinates and the hole radius as

$$\xi = x/a \qquad \eta = y/a \tag{6}$$

The membrane stress resultants are nondimensionalized with respect to a reference membrane stress N_{ref}. The reference stress is chosen depending on the problem: for the axial tension case, the reference stress is chosen to be the membrane stress applied to the shell in the axial direction; for the internal pressure loading case the reference stress is equal to pR, which is the membrane stress in the circumferential direction around the cylinder far from the hole; for the torsion loading problem N_{ref} is chosen to be the membrane shear stress applied to the shell at its outer boundary. The nondimensionalization is carried out so that the two differential equations will emerge with each equation containing a common nondimensional parameter. This condition is met when the nondimensional forms of F and W are given by

$$\bar{F} = F/a^2N_{\text{ref}} \qquad \bar{W} = WEt^2/a^2N_{\text{ref}}[12(1-\nu^2)]^{1/2} \tag{7}$$

where the bar over a quantity denotes its nondimensionality. The complex function Φ, defined as

$$\Phi = \bar{W} - i\bar{F} \tag{8}$$

and the curvature parameter β, defined by Eq. (1), allow the two differential equations (2) and (3) to be combined into the single complex differential equation

$$\nabla^4\Phi + 8i\beta^2\,\Phi_{,\xi\xi} = 8\beta^2 \tag{9}$$

where the right-hand side is present when the shell is loaded by a uniform normal pressure and is zero otherwise.

The uniform states of stress present in the shell before the hole effects are considered may be represented by appropriate nondimensional stress functions $\bar{F}$ for the different loadings considered. For the problem of axial tension,

$$\bar{F} = \eta^2/2 \tag{10}$$

gives the required loading $\bar{N}_{xx} = 1$, and $\bar{N}_{xy} = \bar{N}_{yy} = 0$. For the pressure and torsion loading cases, the stress functions

$$\bar{F} = \eta^2/4 + \xi^2/2 \text{ and } \bar{F} = \xi\eta \tag{11}$$

produce the required stress conditions in the cylinder. For ease in applying boundary conditions, residual problems are formulated by defining new stress functions F^* which are the total stress functions $\bar{F}$ with the stress functions describing the uniform states of stress removed. The constant normal displacements due to the uniform states of stress are removed from the displacements $\bar{W}$, so that the residual displacements W^* are the displacements in the shell due to the presence of the hole. The membrane solutions are then added to the residual problem solutions to obtain total solutions.

By defining the new function Φ^* as

$$\Phi^* = W^* - iF^* \tag{12}$$

the differential equation (9) becomes a homogeneous equation for all loading conditions and is given by

$$\nabla^4\Phi^* + 8i\beta^2\,\Phi^*_{,\xi\xi} = 0 \tag{13}$$

Since the problems concern circular hole boundaries, the boundary conditions must be written for an edge of constant radius. It is therefore useful to introduce the nondimensional polar coordinates defined as

$$\xi = r\cos\theta \qquad \eta = r\sin\theta \tag{14}$$

The equations for the stress resultants and couples become

$$\begin{aligned}
\bar{N}_{,rr} &= \bar{F}_{,r}/r + \bar{F}_{,\theta\theta}/r^2 \qquad \bar{N}_{\theta\theta} = \bar{F}_{,rr} \\
\bar{N}_{r\theta} &= -(\bar{F}_{,\theta}/r)_{,r}
\end{aligned} \tag{15}$$

$$\begin{aligned}
\bar{Q}_r' &= -\{\nabla^2\bar{W}_{,r} + (1-\nu)/r[(1/r)\bar{W}_{,\theta\theta}]_{,r}\} \\
\bar{Q}_\theta' &= -\{(1/r)\nabla^2\bar{W}_{,\theta} + (1-\nu)[(1/r)\bar{W}_{,\theta}]_{,rr}\}
\end{aligned} \tag{16}$$

$$\begin{aligned}
\bar{M}_{rr} &= -\{\bar{W}_{,rr} + \nu[(1/r)\bar{W}_{,r} + (1/r^2)\bar{W}_{,\theta\theta}]\} \\
\bar{M}_{\theta\theta} &= -\{\nu\bar{W}_{,rr} + [(1/r)\bar{W}_{,r} + (1/r^2)\bar{W}_{,\theta\theta}]\} \\
\bar{M}_{r\theta} &= -(1-\nu)[(1/r)\bar{W}_{,\theta}]_{,r}
\end{aligned} \tag{17}$$

where the effective transverse stress terms are defined

$$\bar{Q}_r' = \bar{Q}_r + \bar{M}_{r\theta,\,\theta}/r \qquad \bar{Q}_\theta' = \bar{Q}_\theta + \bar{M}_{r\theta,\,r} \tag{18}$$

The boundary conditions for the total problems are satisfied by requiring that certain stress resultants vanish at the hole. For the three problems, tension, pressure, and torsion, the vanishing of the normal and shearing membrane stresses at the hole for the total problems results in the boundary conditions for the residual problems, at $r = 1$,

$$F^*_{,r} + F^*_{,\theta\theta} = -(1+\cos2\theta)/2,\ (\cos2\theta - 3)/4,\ \sin2\theta \tag{19}$$

$$F^*_{,\theta} - F^*_{,r\theta} = \sin2\theta/2,\ -\sin2\theta/4,\ \cos2\theta \tag{20}$$

Vanishing of the normal stress couples for the total problems requires that, for the residual problems,

$$W^*_{,rr} + \nu(W^*_{,r} + W^*_{,\theta\theta}) = 0,\ 0,\ 0 \tag{21}$$

and vanishing of the effective transverse shear stresses at the hole requires

$$W^*_{,rrr} + W^*_{,rr} - W^*_{,r} + (2-\nu)W^*_{,r\theta\theta} - (3-\nu)W^*_{,\theta\theta} = 0,\ 4\beta^2,\ 0 \tag{22}$$

For the residual problems, the boundary conditions far from the hole may be satisfied by requiring F^* and W^* to be bounded at infinity.

Solution to the Differential Equation

The solution to the differential equation (13), which governs the behavior of the shell, is begun by writing it in the operationally factored form

$$L_1L_2\Phi^* = 0 \tag{23}$$

where

$$L_1 = \nabla^2 - 2(1 - i)\beta(\partial/\partial\xi)$$
$$L_2 = \nabla^2 + 2(1 - i)\beta(\partial/\partial\xi) \quad (24)$$

Since the operators L_1 and L_2 are commutative,

$$\Phi^* = \Phi_1^* + \Phi_2^* \quad (25)$$

where

$$L_1\Phi_1^* = 0 \qquad L_2\Phi_2^* = 0 \quad (26)$$

The operators of Eq. (24) are similar to those encountered by Lamb[7] in a hydrodynamic viscous flow problem, and they may be solved by making separations of the form

$$\Phi_1^* = e^{(1-i)\beta\xi}\psi_1(\xi, \eta) \qquad \Phi_2^* = e^{-(1-i)\beta\xi}\psi_2(\xi, \eta) \quad (27)$$

The functions ψ_1 and ψ_2 then both satisfy the single differential equation

$$\nabla^2\psi + 2i\beta^2\psi = 0 \quad (28)$$

The problems of the shell loaded by axial tension and internal pressure have symmetry about both the ξ and η axes, whereas the torsion problem is antisymmetric about these axes; the solutions in the quadrant where ξ and η are both positive may be continued into the remaining three quadrants by these symmetry properties. It is anticipated that a solution of Eq. (28) may be obtained as the sum of parts that are symmetric and antisymmetric in ξ. Since symmetry and antisymmetry in ξ must be provided by the solutions for Φ^*, it is convenient to combine the functions $e^{(1-i)\beta\xi}$ and $e^{-(1-i)\beta\xi}$ to form new functions that are also symmetric and antisymmetric in ξ. $E_1 - iE_2$, a symmetric combination, is defined as

$$E_1 - iE_2 = [e^{(1-i)\beta\xi} + e^{-(1-i)\beta\xi}]/2 \quad (29)$$

An antisymmetric combination is given by

$$E_3 - iE_4 = [e^{(1-i)\beta\xi} - e^{-(1-i)\beta\xi}](1 + i)/4 \quad (30)$$

These functions are the Krylov functions (Ref. 1, p. 190).

The solutions for the residual problems with symmetry and antisymmetry in ξ become, therefore,

$$\Phi^* = (E_1 - iE_2)\psi_{\text{symm}} + (E_3 - iE_4)\psi_{\text{antisymm}}$$
$$\Phi^* = (E_1 - iE_2)\psi_{\text{antisymm}} + (E_3 - iE_4)\psi_{\text{symm}} \quad (31)$$

For problems symmetric in η as well as ξ, the solution to Eq. (28), written in polar coordinates, is obtained which is symmetric in θ. By separation of variables this solution may be written as the infinite series

$$\psi = \sum_{-\infty}^{\infty} C_n H_n^1[\beta r(2i)^{1/2}] \cos n\theta + \sum_{-\infty}^{\infty} D_n H_n^2 \times [\beta r(2i)^{1/2}] \cos n\theta \quad (32)$$

Since the solutions for Φ^* are to be bounded at infinity, only the parts involving Hankel functions of the first kind H_n^1 will be retained; the Hankel functions of the second kind, which grow exponentially for large arguments, are discarded. Although all the E functions grow exponentially with argument, the Hankel functions of the first kind behave like

$$H_n^1 \sim Ce^{-\beta r}/(\beta r)^{1/2} \quad (33)$$

for large arguments, so that the products of the two have the behavior

$$EH_n^1 \sim Ce^{-\beta r(1-|\cos\theta|)}/(\beta r)^{1/2} \quad (34)$$

By employing the identity

$$H_{-n} = e^{in\pi} H_n \quad (35)$$

the two parts of ψ which were previously assumed to exist become

$$\psi_{\text{symm}} = \sum_{n=0,2,4,\ldots}^{\infty} (A_n + iB_n)H_n^1[\beta r(2i)^{1/2}] \cos n\theta$$
$$\psi_{\text{antisymm}} = \sum_{n=1,3,,\ldots}^{\infty} (A_n + iB_n)H_n^1[\beta r(2i)^{1/2}] \cos n\theta \quad (36)$$

where the unknown real coefficients A_n and B_n are to be determined. For the torsion problem with antisymmetry in η, the $\cos n\theta$ terms become $\sin n\theta$ terms, and the even summation begins with 2.

The method of solution for small values of the curvature parameter, employed originally by Lurie, is expansion of the solution in even powers of β and products of powers of $\ln\beta$ with even powers of β. The known Hankel functions and E functions may be expanded in the parameter β, and similar expansions are made for the unknown coefficients. The boundary conditions will be identically satisfied by every term in the Fourier series solution and also by each term in the expansion series in β and $\ln\beta$. This method was applied originally by Lurie to obtain the membrane stresses at the hole for loading by tension and internal pressure.

At the hole, the circumferential stresses are to be found; they may be written in terms of the nondimensional quantities, for the stresses at the upper and lower faces of the shell, respectively, as

$$\sigma_{\theta\theta} = \bar{N}_{\theta\theta}N_{\text{ref}}/t \pm 6\bar{M}_{\theta\theta}N_{\text{ref}}/t[12(1 - \nu^2)]^{1/2} \quad (37)$$

The stress in the shell far from the hole σ_∞ will be equal to a stress in the shell where there are no hole effects, and this stress has been defined by the reference stress as N_{ref}/t. The ratio of the average stress at the hole $\sigma_{\theta\theta\,\text{av}}$ to the stress in the shell far from the hole will then become

$$\sigma_{\theta\theta\,\text{av}}/\sigma_\infty = \bar{N}_{\theta\theta} \quad (38)$$

where $\sigma_{\theta\theta\text{av}}$ represents the first part of Eq. (37). The maximum bending stress that occurs in the outer fibers of the shell $\sigma_{\theta\theta b}$ represents the second part of Eq. (37). The ratio of this bending stress to the stress far from the hole becomes

$$\sigma_{\theta\theta b}/\sigma_\infty = 6\bar{M}_{\theta\theta}/[12(1 - \nu^2)]^{1/2} \quad (39)$$

and represents either a compressive or tensile stress at the two outer faces of the shell. The stresses in the shell interior are also expressed as the ratio of the actual stress to the stress far from the hole. These stress ratios are given by equations similar to Eqs. (38) and (39), where the dimensionless total

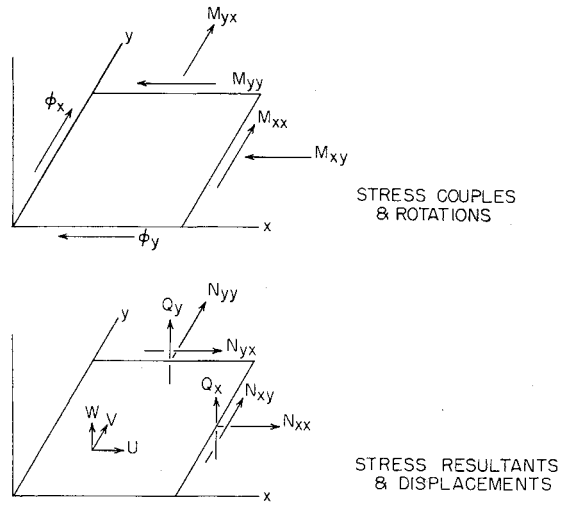

Fig. 2 Stress couples and resultants, rotations, and displacements.

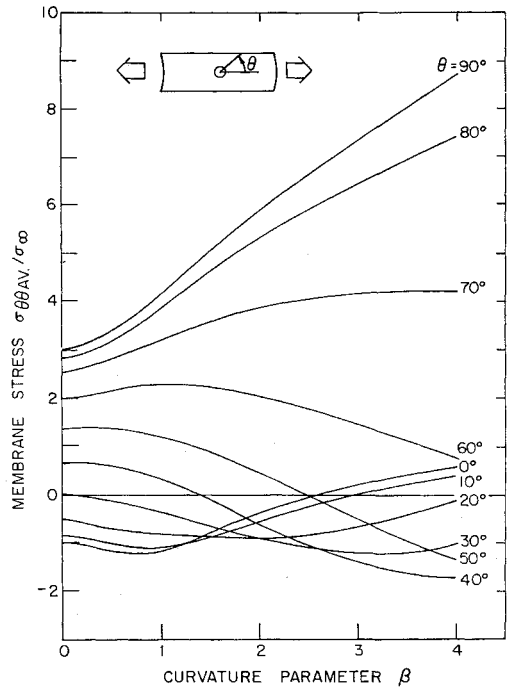

Fig. 3 Membrane stress at the hole under tension loading.

stresses are given in terms of the stress function and the normal displacement by Eqs. (15–17).

The result of the perturbation solution for the membrane stresses in the shell, through terms of order β^2, is

$$\sigma_{\theta\theta_{av}}/\sigma_{\theta\theta} = (1 + r^2)/2r^2 - (3 + r^4)\cos 2\theta/2r^4 - \pi\beta^2(3 + r^4)\cos 2\theta/8r^4 + \ldots \quad (40)$$

for the case of loading by axial tension. For the case of pressure loading, the membrane stresses at the hole $r = 1$ are

$$\sigma_{\theta\theta_{av}}/\sigma_\infty = \tfrac{3}{2} + \cos 2\theta + \pi\beta^2(1 + \tfrac{5}{4}\cos 2\theta) + \ldots \quad (41)$$

for small values of the curvature parameter β. The terms of order β^2 were one-half the values obtained originally by Lurie (Ref. 1, p. 196). These corrections to the starting series results have also been confirmed by Eringen[4] and Lekkerkerker.[5] The results of Shevliakov and Zigel for the torsion loading case are, at the hole $r = 1$,

$$\sigma_{\theta\theta_{av}}/\sigma_\infty = 4(1 + \pi\beta^2/2)\sin 2\theta \quad (42)$$

A Numerical Solution for Loading by Axial Tension

A numerical procedure to obtain the unknown coefficients A_n and B_n was formulated by terminating the series, Eq. (36), at an odd n; there were then $2(n + 1)$ unknown coefficients to be determined. The boundary conditions, Eqs. (19–21), were satisfied by a collocation procedure that enforced them at discrete points on the edge of the hole in the quadrant $\theta = 0$ to $\pi/2$. At each of these boundary points there were four boundary conditions to be satisfied, which gave four equations for the unknown coefficients; $(n + 1)/2$ discrete points were chosen at which to enforce the boundary conditions. The solution of the resulting simultaneous equations determined the coefficients. For this collocation procedure, the points on the boundary were evenly spaced within the quadrant 0 to $\pi/2$. As an example, for a series where n was 9 the five required boundary points were $\pi/12$, $\pi/6$, $\pi/4$, $\pi/3$, and $5\pi/12$. A Poisson's ratio ν of $\frac{1}{3}$ was assumed for the numerical calculations.

For a given β, the infinite series was cut off at successively higher values of n until the values of the calculated functions remained essentially the same for a further increase in the series length. As β was increased, the number of terms needed in the series to obtain converging results also increased. The maximum n used was 27, a series of 28 terms, which resulted in 56 unknown coefficients. The numerical calculations for this procedure were carried out on an IBM 7094 digital computer. Computations of the stress quantities were possible up to a β of 4. For the calculations at β equal to 4 these quantities showed convergence in the longest two series employed, which were 26- and 28-term series; the variation between the values calculated by the two series at various circumferential points was at most about 1%.

The numerical solution was first used to compare the corrected starting series of Lurie, Eq. (40), for the membrane stresses at the hole. Agreement was found to a β of about 0.3; at higher values of β, the starting series is no longer accurate. Figure 3 shows the membrane stresses at the hole obtained over the entire range of β, at 10° intervals around the hole. The bending stresses at the hole, which are given as the ratio of the maximum bending stress in the outer fibers of the shell to the stress in the shell far from the hole, are shown in Fig. 4. The ratio of this bending stress to the membrane stress at the top of the hole, where the membrane stress is a maximum, is shown in Fig. 5; the ratio reaches a maximum of 27.9% at a β of about 3 and begins to decrease for higher values of β. Figure 6 shows some of the interior stresses in the shell. The radial and circumferential membrane and bending stress ratios, for a β of 2, are given for three circumferential positions. As would be anticipated from the behavior indicated by Eq. (34), the stresses due to the hole at the 90° position decay most rapidly.

A Boundary-Layer Analysis for Large β for Loading by Axial Tension

By defining the small parameter

$$\epsilon = 1/\beta \quad (43)$$

the differential equation (13) for the residual problem is

$$\epsilon^2\nabla^4\Phi^* + 8i\Phi^*_{,\xi\xi} = 0 \quad (44)$$

The form of the residual problem solution as β becomes large is thus obtained from Eq. (44) as ϵ goes to zero. The differential equation is factored into two commutative operators, but further separation of the equation is not carried out; they are treated directly by employing boundary-layer techniques. The function Φ_1^* is treated first, and the analogous solution for Φ_2^* may be written directly from these results; the two results are summed by Eq. (25) to obtain the entire residual solution.

The equation for Φ_1^* may be written in polar coordinates as

$$\epsilon\Phi_1^*{}_{,rr} + (\epsilon/r)\Phi_1^*{}_{,r} + (\epsilon/r^2)\Phi_1^*{}_{,\theta\theta} - 2(1 - i)[\cos\theta\Phi_1^*{}_{,r} - (\sin\theta/r)\Phi_1^*{}_{,\theta}] = 0 \quad (45)$$

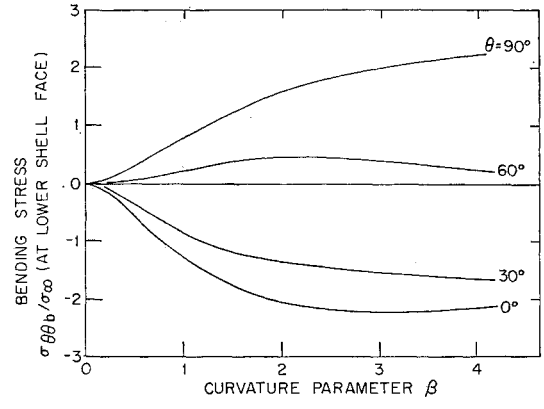

Fig. 4 Maximum bending stress at the hole under tension loading.

The general solution may be written as

$$\Phi_1^* = S(\eta) + iT(\eta) \tag{46}$$

for ϵ equal to zero. The variation from this solution for small values of ϵ will be sought in the form of a boundary layer at the edge of the hole. With the boundary at r equal to a constant, boundary-layer behavior would be expected to occur in a direction normal to the boundary. The radial coordinate is thus scaled by defining

$$\bar{r} = (r - 1)/\epsilon^m \tag{47}$$

where $\bar{r} = 0$ at the hole. The differential equation (45) for Φ_1^* becomes

$$\epsilon^{1-2m}\Phi_1^*{}_{,\bar{r}\bar{r}} + \epsilon^{1-m}(1 - \bar{r}\epsilon^m + \ldots)\Phi_1^*{}_{,\bar{r}} + \epsilon(1 - 2\bar{r}\epsilon^m + \ldots)\Phi_1^*{}_{,\theta\theta} - 2(1 - i)(\epsilon^{-m}\cos\theta\Phi_1^*{}_{,\bar{r}} - \sin\theta(1 - \bar{r}\epsilon^m + \ldots)\Phi_1^*{}_{,\theta}) = 0 \tag{48}$$

The power m is chosen so that the terms from each half of the equation with the most rapid radial variation are retained and so that the remaining terms are of smaller order and may, therefore, be neglected. This implies that m is one, and the first approximation to the transformed equation for Φ_1^* becomes

$$\Phi_1^*{}_{,\bar{r}\bar{r}} - 2(1 - i)\cos\theta\Phi_1^*{}_{,\bar{r}} = 0 \tag{49}$$

Now, at the point where $\cos\theta$ goes to zero, however, the term containing $\cos\theta$ becomes small and is possibly reduced in size to the order of the terms which were previously neglected. The present analysis is, therefore, expected to be valid only in the regions at the sides of the hole where $\cos\theta$ is not zero; a further investigation of the regions at the top and bottom of the hole where $\cos\theta$ is zero must be made.

The solution to Eq. (49) which contains boundary-layer behavior in the radial coordinate is

$$\Phi_1^* = K_{10}(\theta)e^{2(1-i)\bar{r}\cos\theta} + K_{11}(\theta) \tag{50}$$

where K_{10} and K_{11} are functions of θ to be determined by the boundary conditions. This solution is a valid representation of the function Φ_1^*, which is bounded far from the hole, only in the region at the side of the hole where $\cos\theta < 0$ or where $\xi < 0$. In the region where $\cos\theta > 0$, the general solution given by Eq. (46) holds. Φ_1^* then has smooth behavior to the right of the η axis and a possible boundary-layer behavior at the hole to the left of the η axis. The analogous solution for Φ_2^* is written as

$$\Phi_2^* = K_{20}(\theta)e^{-2(1-i)\bar{r}\cos\theta} + K_{21}(\theta) \tag{51}$$

This solution has smooth behavior to the left, and a possible boundary layer to the right of the η axis. The total solution is, therefore,

$$\Phi^* = K_{20}(\theta)e^{-2(1-i)\bar{r}\cos\theta} + K_{21}(\theta) + S(\eta) + iT(\eta) \qquad \xi > 0 \tag{52}$$

$$\Phi^* = K_{10}(\theta)e^{2(1-i)\bar{r}\cos\theta} + K_{11}(\theta) + S(\eta) + iT(\eta) \qquad \xi < 0$$

where the unknown coefficients, functions of θ, are complex.

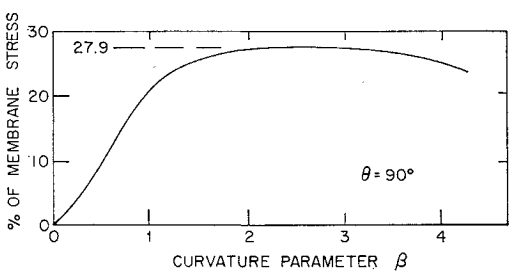

Fig. 5 Ratio of bending to membrane stress at the point of maximum membrane stress under tension loading.

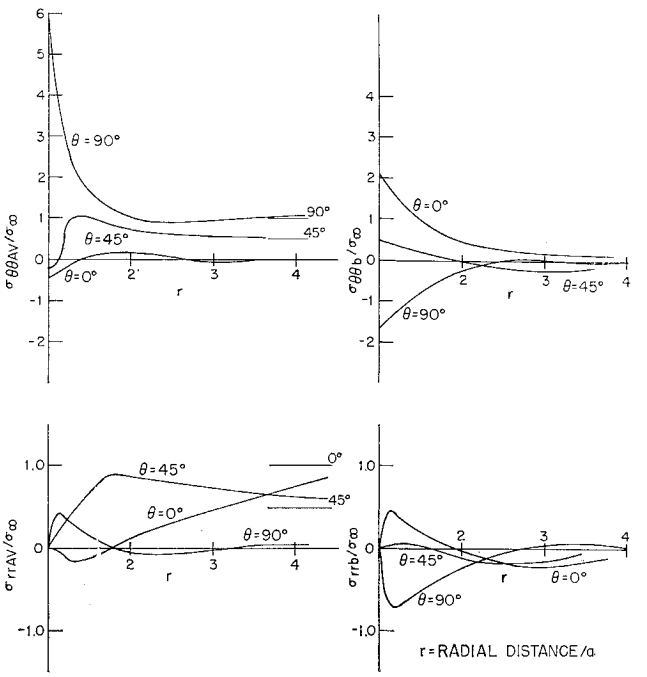

Fig. 6 Interior stresses for $\beta = 2$ under tension loading.

The boundary conditions are changed by the scaling of Eq. (47), and become, at $\bar{r} = 0$,

$$W^*{}_{,\bar{r}\bar{r}\bar{r}} = W^*{}_{,\bar{r}\bar{r}} = 0 \qquad F^* = K_1(\beta) - \sin^2\theta/2$$
$$\bar{F}^*{}_{,\bar{r}} = -\epsilon\sin^2\theta \tag{53}$$

The boundary conditions on the stress function and its derivative are obtained by integrating the boundary conditions of Eqs. (19) and (20). The presence of the homogeneous boundary conditions on $W^*{}_{,\bar{r}\bar{r}\bar{r}}$ and $W^*{}_{,\bar{r}\bar{r}}$ implies that the coefficients K_{10} and K_{20} are zero. There is, then, no boundary-layer behavior at the hole sides, and the solution for Φ^* which satisfies the boundary conditions may be written as the smooth function

$$\Phi^* = K_3 + i\eta^2/2 - iK_1(\beta) \tag{54}$$

This solution for Φ^* implies that the region at the sides of the hole forms a "dead region" that is devoid of stress; the total solution for the stress function $\bar{F}$ is the constant K_1 which does not produce any stresses. The tendency of the membrane stresses at the sides of the hole to die out for increasing β may be seen in Fig. 3; the "dead region" with no stresses is beginning to form. The second boundary condition of Eqs. (53) implies that all of the circumferential bending stress resultants at the hole will eventually become zero for small ϵ; the bending stresses of Fig. 4 have, in most cases, reached maximum values and started to decrease in magnitude. The conjectured boundary layer, which did not prove to exist, is shown as the regions 1 in Fig. 7. Region 3 represents the region where the smooth behavior, present when ϵ is zero, is assumed to exist; this smooth region extends to the hole edge for the axial tension loading case and is the "dead region" which has been described.

Because of the possibility of a different type of behavior at the top and bottom of the hole, at $\theta = \pi/2$ and $\theta = -\pi/2$, a different coordinate expansion is now made in these regions. A scaling in the two directions is made by

$$\bar{y} = (r - 1)/\epsilon^m \qquad \bar{x} = a/\epsilon^p \qquad a = \pi/2 - \theta \tag{55}$$

The $\bar{x}$ axis represents the hole edge, the $\bar{y}$ direction is perpendicular to the boundary, and the origin of the new coordinate system is at the top of the hole at its edge. The differ-

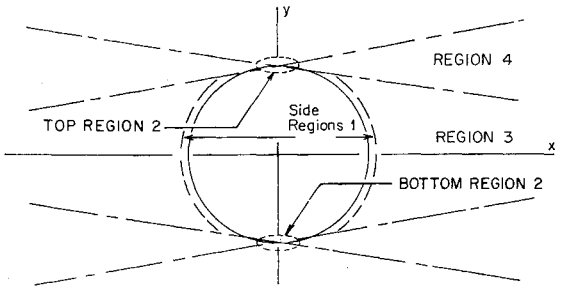

Fig. 7 Boundary-layer regions.

ential equation (45) becomes

$$\epsilon^{1-2m}\Phi_1^*{}_{,\bar{y}\bar{y}} + \epsilon^{1-m}(1 - \bar{y}\epsilon^{-m} + \ldots)\Phi_1^*{}_{,\bar{y}} + \epsilon^{1-2p}(1 - 2\bar{y}\epsilon^{-m} + \ldots)\Phi_1^*{}_{,\bar{x}\bar{x}} - 2(1-i) \times [(\bar{x}\epsilon^p + \ldots)\epsilon^{-m}\Phi_1^*{}_{,\bar{y}} + (1 - \bar{y}\epsilon^{-m} + \ldots) \times (1 - \bar{x}^2\epsilon^{2p}/2 + \ldots)\epsilon^{-p}\Phi_1^*{}_{,\bar{x}}] = 0 \quad (56)$$

Now, to retain terms with the most rapid variation in the two coordinates from both halves of the original equation, the powers m and p become $\frac{2}{3}$ and $\frac{1}{3}$, respectively. The terms ϵ^{1-m} and ϵ^{1-2p} are of the same order $\epsilon^{1/3}$ and are neglected in comparison with the $\epsilon^{-1/3}$ order terms. The first approximation equations that result for the two functions are, therefore,

$$\Phi_1^*{}_{,\bar{y}\bar{y}} - 2(1-i)(\bar{x}\Phi_1^*{}_{,\bar{y}} + \Phi_1^*{}_{,\bar{x}}) = 0$$
$$\Phi_2^*{}_{,\bar{y}\bar{y}} + 2(1-i)(\bar{x}\Phi_2{}_{,\bar{y}}{}^* + \Phi_2^*{}_{,\bar{x}}) = 0 \quad (57)$$

The total equation for Φ^* may be written

$$\Phi^*{}_{,\bar{y}\bar{y}\bar{y}} + 8i(\Phi^*{}_{,\bar{x}\bar{x}} + \bar{x}^2\Phi^*{}_{,\bar{y}\bar{y}} + 2\bar{x}\Phi^*{}_{,\bar{x}\bar{y}} + \Phi^*{}_{,\bar{y}}) = 0 \quad (58)$$

The solution to this equation is sought which is bounded away from the hole and satisfies the boundary conditions at the hole, $\bar{y} = 0$,

$$W^*{}_{,\bar{y}\bar{y}\bar{y}} = W^*{}_{,\bar{y}\bar{y}} = 0$$
$$F^* = K_1 - \tfrac{1}{2} + \bar{x}^2\epsilon^{2/3}/2 + \ldots \quad (59)$$
$$F^*{}_{,\bar{y}} = -\epsilon^{2/3} + \ldots$$

Regions 2 of Fig. 7 are the boundary layers at the top and bottom of the hole. In addition, the figure shows a region 4, which is an expected interior boundary-layer area that will connect the smooth behavior in region 3 with the conditions in the shell far from the hole.

This first approximation to the behavior of the stresses for small values of ϵ again indicates that the circumferential bending stress resultant at the top of the hole will be zero, by the second boundary condition of Eq. (59). The circumferential membrane stress at the hole will, however, be given by

$$\sigma_{\theta\theta\mathrm{av}}/\sigma_\infty = \bar{N}_{\theta\theta} = \epsilon^{-4/3}F^*{}_{,\bar{y}\bar{y}} + 1 \quad (60)$$

where the scaling of the r coordinate has been applied to Eq. (15). Since the required stresses are independent of a constant in the stress function F^*, the quantity $K_1 - \frac{1}{2}$ may be dropped from the boundary conditions. These new boundary conditions then imply a solution for F^* of the form

$$F^* = L(\bar{x}, \bar{y})\epsilon^{2/3} \quad (61)$$

and this gives, by Eq. (60),

$$\sigma_{\theta\theta\mathrm{av}}/\sigma_\infty = \epsilon^{-2/3}K_T + 1 \quad (62)$$

for the point at the top of the hole at the hole edge. Anticipating this form for the membrane stresses at the top of the hole, the data from the intermediate β calculation may be presented as shown in Fig. 8. From this figure it appears that K_T will have a value very near 3.05, and the membrane stresses may then be written

$$\sigma_{\theta\theta\mathrm{av}}/\sigma_\infty \approx 3.05\beta^{2/3} + 1 \quad (63)$$

at the top of the hole, $\theta = \pi/2$, for large values of the curvature parameter β. The exact solution of the boundary value problem, represented by the differential equation (58) and the boundary conditions (59), was found to be very difficult to obtain; it was also felt that a very accurate determination of the solution to this system would be necessary in order to improve the estimate represented by Eq. (63).

Loading by Internal Pressure and Torsion

As in the axial tension case, the starting series for small β, given by Eq. (41) for pressure loading, is generally accurate to a β of about 0.3. Figure 9 shows the membrane stresses at the hole obtained over the entire β range. The stresses at 0° and 10° around the hole appear to have reached peak values, but then they begin to increase again; all of the stresses appear to be increasing at the upper limit of the calculations, where β is about 4. The bending stresses of Fig. 10 are much higher in magnitude than in the axial tension case; however, it is anticipated that at higher values of β these stresses will drop off as the membrane stresses continue to rise. The stresses in the interior of the shell are shown in Fig. 11. The stresses due to the hole at the top of the shell, where θ is $\pi/2$, decrease rapidly as the radial distance from the hole

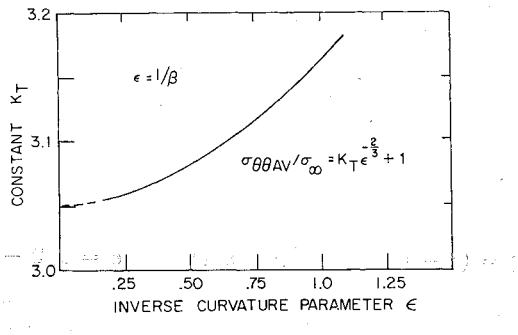

Fig. 8 Membrane stress at top of hole for large β under tension loading.

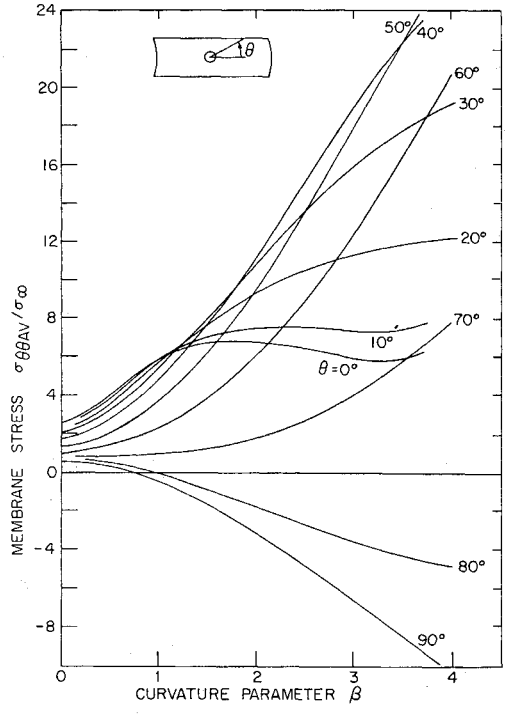

Fig. 9 Membrane stress at the hole under pressure loading.

increases. The convergence of the numerical calculations was slightly less than that obtained from the previous problem; at a β of 3.5, the largest variation in the stresses calculated by the longest two series was about 2%.

The nature of the boundary layer for the problem of loading under internal pressure is altered from that of the tension loading problem. At the sides of the hole, the same scaling of coordinates implies a possible boundary layer and smooth behavior of the form of Eq. (52). The boundary conditions are, at $\bar{r} = 0$,

$$W^*_{,\bar{r}\bar{r}\bar{r}} = 4\epsilon \qquad W^*_{,\bar{r}\bar{r}} = 0$$
$$F^* = K_2 - \tfrac{1}{2} + \sin^2\theta/4 \qquad F^*_{,\bar{r}} = \epsilon\,(\sin^2\theta/2 - 1) \tag{64}$$

where again the boundary conditions on the stress function and its derivative are obtained from Eqs. (19) and (20) by integration. For the internal pressure case, these boundary conditions do allow a boundary-layer behavior at the sides of the hole which will merge with a smooth behavior away from the hole edge. The solution for the residual problem function Φ^* may be written

$$\Phi^* = \epsilon e^{-2(1-i)\bar{r}\cos\theta/4}\cos^3\theta + i(\ln\tan^2\theta/4 + \tfrac{1}{2} - \ln\sin\theta) + K(\theta) + i\{4\ln\eta - \eta^2 - [\ln\eta^2/(1-\eta^2)]\}/4 + S(\eta) \qquad \xi > 0 \tag{65}$$

The boundary layer represented by the first term of this equation has a thickness of order $a/\cos\theta$. The boundary conditions continue to imply that for small values of ϵ the circumferential bending stress resultant at the edge of the hole will be zero. The circumferential membrane stress resultant at the hole edge is, however, for $|\cos\theta| > 0$,

$$\bar{N}_{\theta\theta} = 2\beta/|\cos\theta| + (\cos 2\theta + 3)/4 \tag{66}$$

This result may be interpreted physically by considering the circumferential membrane stress, acting over the width of the boundary layer, to be balancing the effective transverse shear acting at the edge of the hole. The projected connection between the calculated circumferential membrane stresses at the sides of the hole and this large β behavior is shown in Fig. 12. Again, however, this behavior is only valid at the sides of the hole, and a different analysis must be made for the points at the top and bottom of the hole.

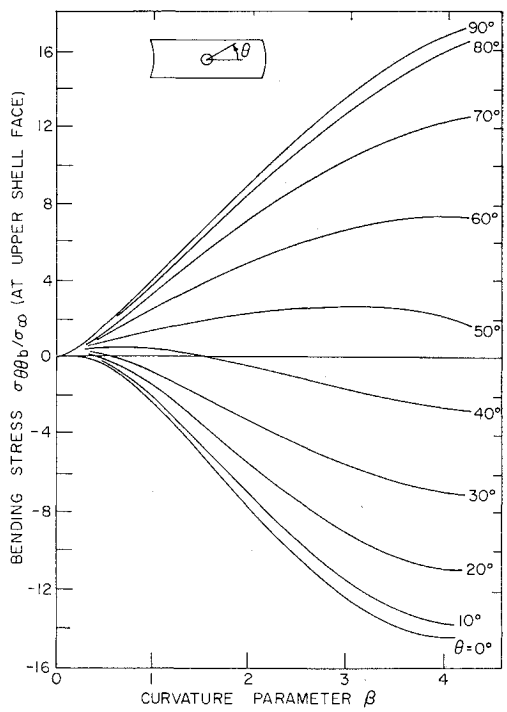

Fig. 10 Maximum bending stress at the hole under pressure loading.

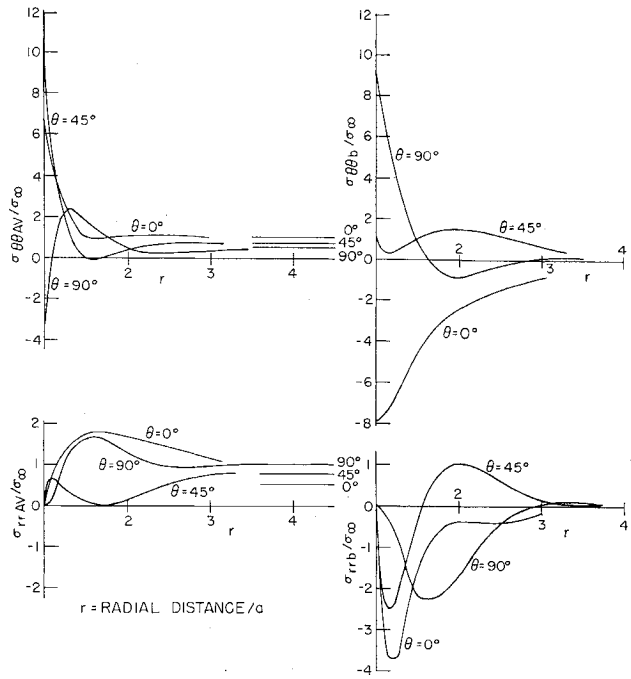

Fig. 11 Interior stresses for $\beta = 2$ under pressure loading.

For these regions at the top and bottom of the hole the boundary conditions at $\bar{y} = 0$ become

$$W^*_{,\bar{y}\bar{y}\bar{y}} = 4 \qquad W^*_{,\bar{y}\bar{y}} = 0$$
$$F^* = K_2 - \tfrac{3}{4} + \bar{x}^2\epsilon^{2/3}/4 + \ldots \tag{67}$$
$$F^*_{,\bar{y}} = -\epsilon^{2/3}/2 + \ldots$$

The differential equation to be solved for the boundary-layer behavior is still Eq. (58). As a first approximation to the solution for small ϵ, all of the boundary conditions except for the constant transverse shear stress may be considered to be zero. These boundary conditions then imply a solution that is of order one, and the scaling of coordinates at the top of the hole gives the circumferential membrane stress resultant at the hole edge for the total problem as

$$\bar{N}_{\theta\theta} = K_p\epsilon^{-4/3} + \tfrac{1}{2} \tag{68}$$

Again, the circumferential bending stress resultant at the hole edge vanishes. By anticipating this form for the membrane stresses at the top of the hole, where $\theta = \pi/2$, the intermediate β data gives, as shown in Fig. 13, the approximate

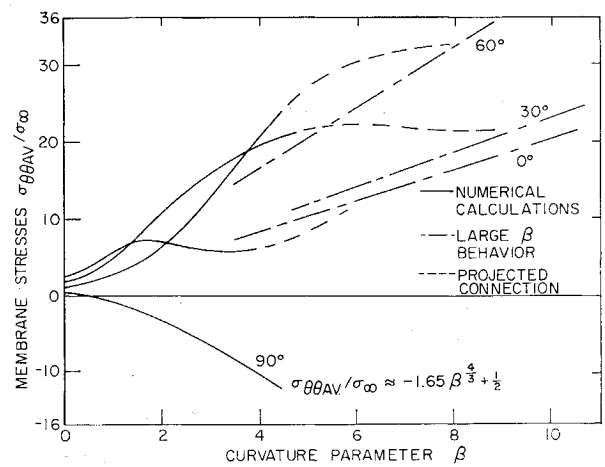

Fig. 12 Membrane stress at top of hole for large β under pressure loading.

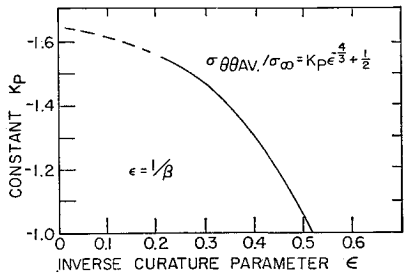

Fig. 13 Projected membrane stresses for large β under pressure loading.

expression

$$\sigma_{\theta\theta av}/\sigma_\infty \approx -1.65\beta^{4/3} + \tfrac{1}{2} \tag{69}$$

for large values of the curvature parameter β.

The problem of the torsion loading of the shell requires use of the antisymmetric system of equations; the series solution of Eq. (36) was terminated on an even n to give $2n$ equations; the boundary conditions were enforced at $n/2$ points on the edge of the hole in the collocation procedure. The selection of these points, which lie in the quadrant $\theta = 0$ to $\pi/2$, was identical with that outlined for the previous cases. For small values of β the numerical results are identical with the starting series of Shevliakov and Zigel, Eq. (42), to a β of 0.3. All of the results of calculations for the membrane stresses at the hole are given in Fig. 14; it is seen that the point of maximum stress is moving toward the top of the hole as β is increased. The values of the stresses are increasing for points toward the top of the hole, whereas for points at the side of the hole the stresses have reached peak values and are starting to decrease. The bending stresses shown in Fig. 15 demonstrate somewhat similar behavior in that the stresses at the top of the hole are increasing whereas those at the sides have begun to show signs of leveling off. Some of the interior stresses are shown in Fig. 16, where the stresses near the top of the hole show the most rapid decay to their values away from the hole. The convergence for the torsion problem was comparable to that obtained in the case of loading by axial tension; at a β of 4, the largest variation in calculated stresses for the longest two series was about 2%.

The boundary-layer analysis that lent itself with such facility to the problems of loading by tension and internal pressure proves to be less easily applied to the problem of loading by torsion. The absence of an effective transverse shear or stress couple at the hole precludes the presence of a boundary layer at the hole edge at the sides, and the antisymmetry of the problem implies the absence of a membrane stress resultant at the top or bottom of the hole. Figure 14 illustrates the fact that the maximum stress is increasing with an increase in the parameter β and that this point of maximum stress is approaching the top of the hole. As can be seen from the points at 50° to 60° on the hole, the stresses in the upper regions of the hole rise to a point where they represent the maximum stress but they then fall off in magnitude. A more detailed boundary-layer analysis might well illustrate the position and behavior of the maximum stress as the inverse parameter ϵ becomes small. The boundary conditions on the normal bending stress resultant at the hole edge will again, as ϵ becomes small, eliminate the circumferential bending stress resultant at the hole edge; Fig. 15 indicates that some of the bending stresses are beginning to level off in magnitude.

Results and Conclusions

The determination of stresses occurring around holes in cylindrical shells by experimental techniques has been a topic of some recent interest, partly due to the previous unavailability of theoretical solutions beyond those for small values of the curvature parameter. A summary of the experimental results is given in Fig. 17 where comparisons are made with the theoretical solutions. The experimental results are those of Jessop, Snell, and Allison[8] on tubes of inside to outside diameter ratio of 0.9 loaded in axial tension and torsion; the results of Houghton[9] where frozen stress techniques were used on Araldite B shell models loaded in axial tension, internal pressure, and torsion; and the larger series reported by Houghton and Rothwell[10] where additional tests were run on aluminum alloy panels under the three loadings with the stresses measured with electrical strain gages. In all of these experiments only the membrane stresses were measured, and the results were presented as maximum direct stress concentrations. These stress concentrations correspond to the ratio of the circumferential membrane stress at the hole to the stress in the shell far from the hole.

The best agreement between experiments and theory is shown by the torsion loading case, as indicated by Fig. 17. Also, the change in position of the point of maximum stress was noted by Houghton and Rothwell in the report of the experiments for the torsion case, but for the range of curvature parameter covered by the experiments this change is slight and the point of maximum stress is essentially the same as it is for the flat plate. For the internal pressure case rather good agreement is shown between the two experimental points and the theoretical solution, as shown in Fig. 17. The boundary conditions at the hole, which are assumed by the theoretical solution, could have been realized by covering the hole with a flexible membrane that would have allowed the hole edge to twist and deflect freely while applying a uniform transverse shear to the edge of the hole. The experimental system, however, consisted of a very flexible, thin metal plug covering the hole, and this might have introduced slight restraints on the freedom of the hole edge. In the paper presented by Lekkerkerker,[5] some experiments are also described; comparisons with the theoretical results are presented for the torsion loading case for the stresses in the shell interior as well as the hole edge.

Comparisons with the theoretical results of Withum, Lekkerkerker, and Eringen for the stresses at the hole and in the

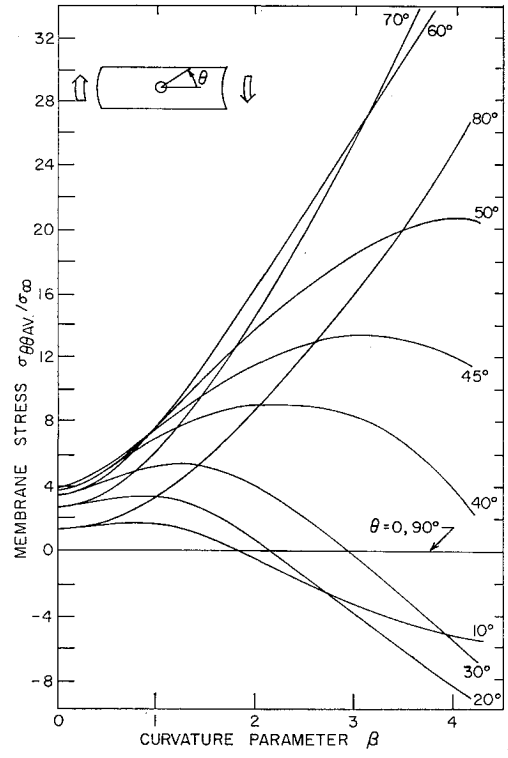

Fig. 14 Membrane stress at the hole under torsion loading.

shell interior were made, and all results were in agreement, with the exception of the circumferential bending stresses reported by Eringen. As may be seen from Figs. 6, 11, and 16, these bending stresses have the same decaying characteristics of the other stresses.

The question of the range of applicability of the shallow shell theory can now be discussed, with the exponential decay of the hole effects in the circumferential direction around the shell

$$EH_n^1 \sim Ce^{-\beta r}/(\beta r)^{1/2} \tag{70}$$

obtained from Eq. (34) for $\theta = \pi/2$ or $-\pi/2$. A shallow shell may be characterized as one whose ratio of rise to base length $\delta/2\tilde{y}$ is not greater than about $\frac{1}{8}$. The middle surface of the shallow shell is represented by a parabolic surface, and this implies a shallowness criterion that the base length $2\tilde{y}$ is less than the radius of curvature R. The first consideration is that the hole itself lie within the shallow shell region. This implies a shell base length equal to $2a$, and the shallowness criterion implies that

$$a/R < \tfrac{1}{2} \tag{71}$$

for the hole to lie within the shallow region. A correction to this requirement will be made by considering the decay of the hole effects of Eq. (70). The hole effects will be considered to have died out when they have been reduced to one-tenth of their original value. Denoting the nondimensional distance to the point where this decay has taken place by $\bar{r}$, the relationship between the parameter β and $\bar{r}$ may be written

$$e^{-\beta(\bar{r}-1)}/(\bar{r})^{1/2} = \tfrac{1}{10} \tag{72}$$

By employing the shallowness criterion, the definition of β, and noting that $\tilde{y} = a\bar{r}$, the region of applicability of shallow, thin shell theory may be determined, as shown in Fig. 18. For large values of β, corresponding to small values of t/R, the exponential decay of Eq. (72) may be considered to be dominant; a value of the exponent equal to 2.3 will then produce the required decay. The region of applicability of the shallow shell theory may then be defined by the equation

$$a/R < \beta/(4.6 + 2\beta) \tag{73}$$

for large values of β. This equation, written in terms of the definition of β, with $\nu = \frac{1}{3}$, becomes

$$a/R < \tfrac{1}{2} - 3.6(t/R)^{1/2} \tag{74}$$

This represents the correction to the requirement that just the hole lie within the shallow region of the shell. Equation (74) defines the region of validity of shallow shell theory only for small values of the thickness ratio t/R, as shown by the dotted boundary line in Fig. 18.

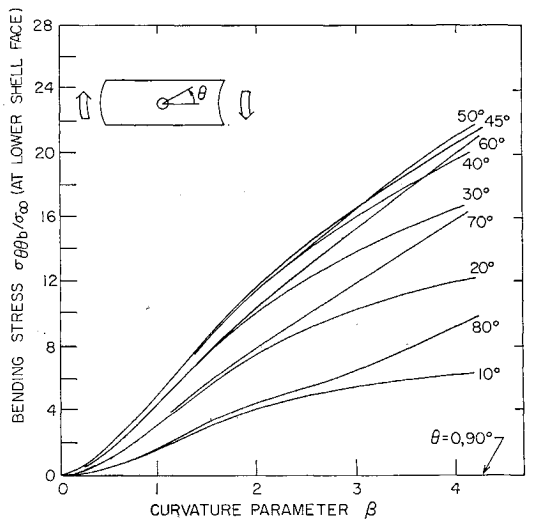

Fig. 15 Maximum bending stress at the hole under torsion loading.

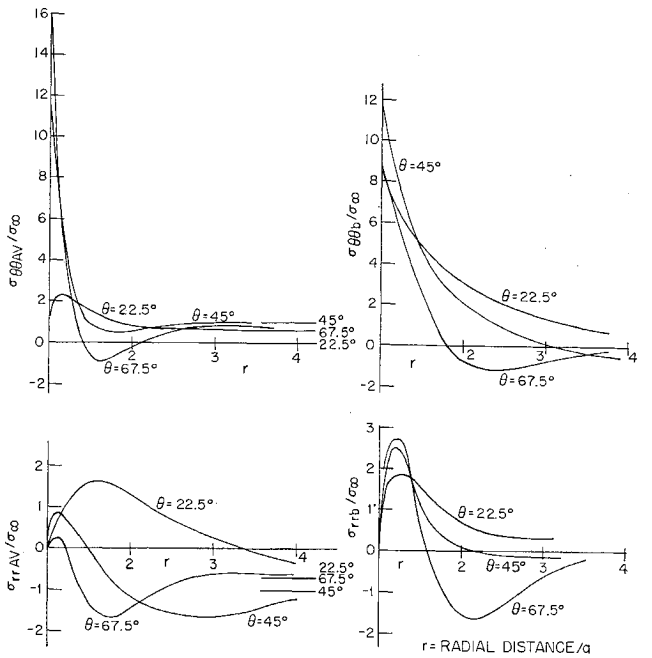

Fig. 16 Interior stresses for $\beta = 2$ under torsion loading.

The numerical calculation procedure is a logical continuation of the solution to the problem with the solution written as an infinite series. High-speed computers make extensive calculations and determination of approximation errors feasible. These numerical calculations serve not only as a source of numbers, however, but also indicate the trends of the stresses as the curvature parameter β becomes large. In the cases of loading by axial tension and internal pressure, the behaviors of the circumferential membrane stresses at the top of the hole for large values of β were correlated with the intermediate β numerical calculations. A conclusive step in the large β analysis would be the exact solution of

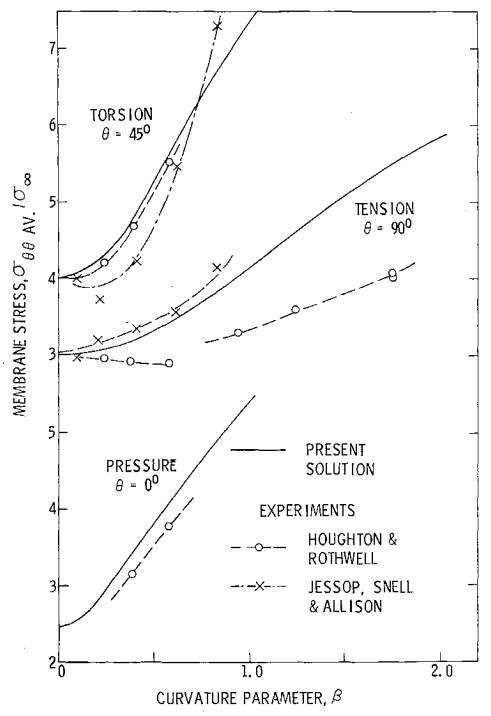

Fig. 17 Experimental results.

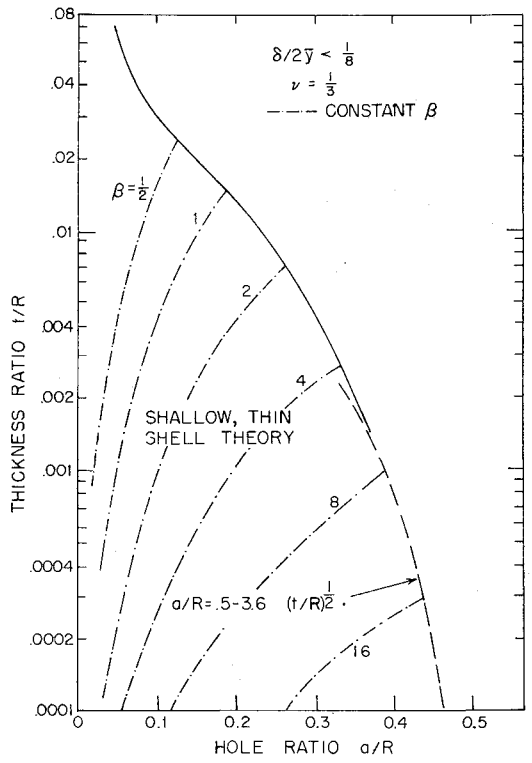

Fig. 18 Region of validity of shallow shell theory.

the boundary value problem which determines the stress behavior at the top of the hole for loading by tension and internal pressure. Further work on the entire boundary-layer analysis for the case of torsion loading would also prove valuable so that better descriptions of the stress behaviors which were noted in the calculated data might be obtained.

References

[1] Lurie, A. I., *Statics of Thin-Walled Elastic Shells* (State Publishing House of Technical and Theoretical Literature, Moscow, 1947), transl.; also Atomic Energy Commission AEC-TR-3798, pp. 147–200 (1959).

[2] Shevliakov, I. A. and Zigel, F. S., "The torsion of an empty cylinder with a hole in its side surface," Dopovidi Ann. U.S.S.R. **1**, 41–44 (1954).

[3] Withum, D., "The cylindrical shell with a circular hole under torsion," Ingr.-Arch. **26**, 435–446 (1958).

[4] Dixon, R. C., Eringen, A. C., Jordan, N. F., Kline, L. V., Koh, S. L., Naghdi, A. K., and Thiel, C. C., "Reports on stresses and stress concentrations in a circular cylindrical shell with a circular cutout," General Technology Corp., TR 3-1, 3-2, 3-3, and 3-4 (August 1961 to June 1963).

[5] Lekkerkerker, J. G., "Stress concentration around circular holes in cylindrical shells," *Proceedings of the Eleventh International Congress of Applied Mechanics 1964* (Springer-Verlag, Berlin, Germany, to be published).

[6] Marguerre, K., "Zur Theorie der gekrümmten Platte grosser Formänderung," *Proceedings of the Fifth International Congress of Applied Mechanics* (John Wiley and Sons, Inc., New York, 1938), pp. 93–99.

[7] Lamb, H., *Hydrodynamics* (Dover Publications Inc., New York, 1932), 6th ed., Chap. XI, p. 615.

[8] Jessop, J. T., Snell, C., and Allison, I. M., "The stress concentration factors in cylindrical tubes with transverse circular holes," Aeron. Quart. **10**, 326–344 (1959).

[9] Houghton, D. S., "Stress concentration around cut-outs in a cylinder," J. Roy. Aeron. Soc. **65**, 201–204 (1961).

[10] Houghton, D. S. and Rothwell, A., "The effect of curvature on the stress concentration around holes in shells," The College of Aeronautics, Cranfield, England, Rept. 156 (May 1962).